Available online at www.sciencedirect.com

SciVerse ScienceDirect

Ceramics International 38 (2012) 5889–5896

CERAMICS INTERNATIONAL

www.elsevier.com/locate/ceramint

Extrinsic behavior in $La_{0.67}Ca_{0.33}MnO_3$–$BaTiO_3$ composites

Leena Joshi *, Sunita Keshri

Department of Applied Physics, Birla Institute of Technology, Mesra, Ranchi 835215, India

Received 11 February 2012; received in revised form 12 April 2012; accepted 12 April 2012
Available online 25 April 2012

Abstract

A manganite matrix based nano-composite series, $(1-x)La_{0.67}Ca_{0.33}MnO_3$(LCMO)–$(x)BaTiO_3$(BTO), has been prepared by the pyrophoric method. Influence of BTO phase on structural and magneto-transport properties of LCP phase has been studied using structural and transport investigations. The series exhibits a conduction threshold at $x_m \sim 0.30$. Overall pattern of temperature dependence of resistivity for this series has been fitted with a percolation model. Almost 200% improvement has been observed by the formation of composite when compared to the parent sample.

© 2012 Elsevier Ltd and Techna Group S.r.l. All rights reserved.

Keywords: CMR-based composites; Grain boundaries; Extrinsic and intrinsic MR; M–I transition

1. Introduction

Considerable attention in the recent past has been paid worldwide to the studies of perovskite manganites owing to their exhibition of colossal magnetoresistance (CMR) and other novel properties [1]. For practical application of CMR materials a large magnetoresistance (MR) at low magnetic field range is often desired over a wide temperature. The MR at low temperature arises mainly because of grain boundary (GB) effects related to the natural and artificial GBs [2]. This is because of the fact that the Mn–O–Mn bond angles responsible for the double exchange (DE) mechanism gets altered by any structural disorder near the GB. These disorders include vacancies, dislocations, oxygen non-stoichiometry, termination of crystal structure, etc. [3,4]. The spin disorders produce strong scattering center for high spin polarized conduction electrons around GBs and are responsible for a high zero-field electrical resistance. When a magnetic field is applied, it can align the originally disordered Mn spins, thus reducing the scattering and leading to an increase in MR. One possible route to obtain large MR under low fields is to utilize GBs for the effect of spin-polarized tunneling through CMR/insulator/CMR structures below ferromagnetic (FM) to paramagnetic (PM) transition temperature (T_c). Recently, several groups have reported enhancement of MR by preparing composites containing CMR material and a secondary phase. Such attempts include $La_{0.67}Ca_{0.33}MnO_3$ (LCP)–$BaTiO_3$ (BTO) [5], $La_{0.67}Ca_{0.33}MnO_3$–$CuMn_2O_4$ [6], $La_{0.67}Ca_{0.33}MnO_3$–MgO [7], $La_{0.7}Sr_{0.3}MnO_3$–Ta_2O_5 [8], $La_{0.7}Pb_{0.3}MnO_3$–SiO_2 [9], $La_{0.7}Sr_{0.3}MnO_3$–$CuCrO_2$ [10], $Pr_{0.67}Ba_{0.33}MnO_3$–$Pr_{0.67}Sr_{0.33}MnO_3$ [11], etc. Moreover, such composites composed of two different small-sized (preferably nanometer-sized) crystallites may possess more enhanced MR because of significantly higher contact area between the two constituent compounds [12]. Hence attempts have been taken to explore the behaviors of such composites with nano grain sizes [6,10].

In our previous paper, we have reported the electrical and magnetic properties of micro-sized LCP-BTO [5] series which had a peaky intrinsic MR behavior at T_c followed by a wide extrinsic MR behavior below this temperature. Our main motivation behind the present investigation is to study the effect of change in MR because of reduction of grain size of matrix as well as second phase.

2. Experimental details

The polycrystalline composite series of $(1-x)$LCP(x)BTO, where $x = 0.0$, 0.10, 0.20, 0.30 and 0.40, were prepared in two steps. Firstly, single phase LCP was prepared by pyrophoric (PY) method as described elsewhere [13]. The advantage of this technique is the smaller particle size, good particle size distributions, good compositional control and low sintering

* Corresponding author.
E-mail address: leenaljoshi@gmail.com (L. Joshi).

0272-8842/$36.00 © 2012 Elsevier Ltd and Techna Group S.r.l. All rights reserved.
http://dx.doi.org/10.1016/j.ceramint.2012.04.040

temperature. It was then mixed with fine powder of BTO prepared using PY method in required ratio and pressed into pellets. The pellets were finally sintered at 900 °C in air for 2 h, and then slowly furnace cooled to room temperature.

The structural characterization was carried out by employing the X-ray diffraction (XRD) technique at room temperature using Cu K_α radiation in the range $20^\circ \leq 2\theta \leq 80^\circ$ with a step size of 0.02. The surface morphology of the samples was observed by JEOL scanning electron microscope (SEM); equipped with Oxford INCA energy dispersive X-ray (EDX) spectrometer. AC susceptibility measurements were carried out with the variation of temperature down to 100 K where real and imaginary components were resolved using a Stanford lock-in-amplifier. DC electrical resistivity as a function of temperature down to 5 K was measured using the standard four-probe technique with an accuracy of ±0.05 K. A magnetic field of 3 T was applied to measure the MR effect, using a 7 T superconducting magnet.

3. Results and discussion

3.1. Structural and microscopic analysis

3.1.1. XRD analysis

The phase purity and lattice parameters of the synthesized samples were examined by means of powder XRD at room temperature. Fig. 1 shows the XRD patterns of all composite samples as well as both parent samples. Using 'Checkcell' software we have found that LCP has an orthorhombic structure with *Pnma* space group whereas BTO has a tetragonal structure with *P422* space group. It can be seen from this figure that for composite samples, the diffraction peaks caused by the individual phases are distinguishable from each other. No additional peak of any other phase is observed, indicating that the chance of interdiffusion between both phases is negligible. The calculated parameters have been listed in Table 1. It can be seen from the table that there is no significant change in the lattice parameters because of presence of BTO. It is thereby believed that the composites of this series consist of two chemically separated phases.

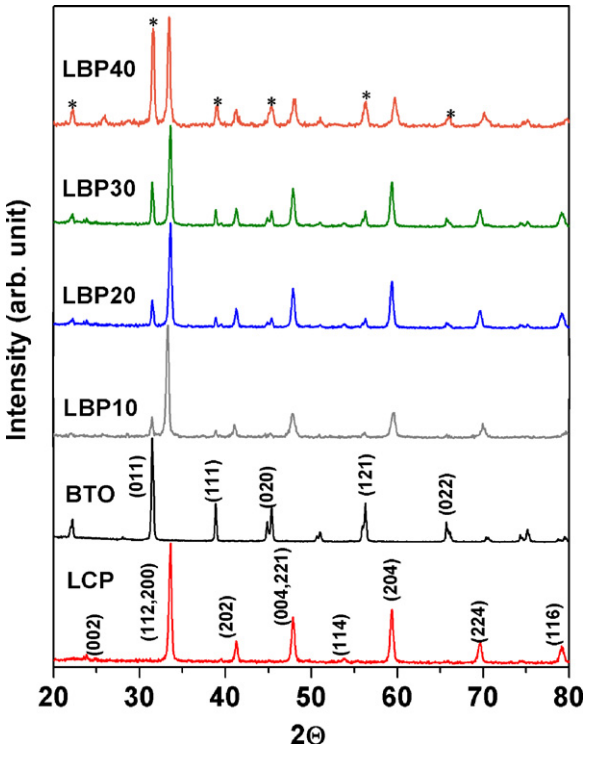

Fig. 1. XRD patterns for LCP, LBP10, LBP20, LBP30 and LBP40; the peaks due to BTO are marked with "*".

Table 1
Parameters of LBP composite series.

Sample (Å)	a (Å)	b (Å)	c (Å)	T_c (K)	T_{MI} (K)
LCP	5.46(1)	5.47(1)	7.70(2)	270	232
LBP10	5.45(1)	5.46(2)	7.71(1)	268	126
LBP20	5.43(2)	5.45(1)	7.72(2)	268	125
LBP30	5.44(2)	5.46(2)	7.72(1)	267	114
LBP40	5.44(3)	5.46(1)	7.71(3)	267	134
BTO	3.98(2)	3.98(1)	4.03(1)		

3.1.2. FTIR analysis

The IR transmission spectra of the complete series measured at room temperature is shown in Fig. 2. The FTIR spectrum of the LCP sample shows a major absorption band at 594 cm^{-1}. This band arises due to vibrating modes of MnO_6 octahedra. Similar band around 600 cm^{-1} has been observed by Kolat et al. also [14]. BTO shows two absorption bands in the ranges of 600–470 and 470–375 cm^{-1}, due to vibration modes of TiO_6 octahedraon [15]. IR spectra of composite samples contain no other additional peak than the absorption bands of both the phases. It can be observed that the peak width of composite samples at ~594 cm^{-1} increase with BTO addition but no peak

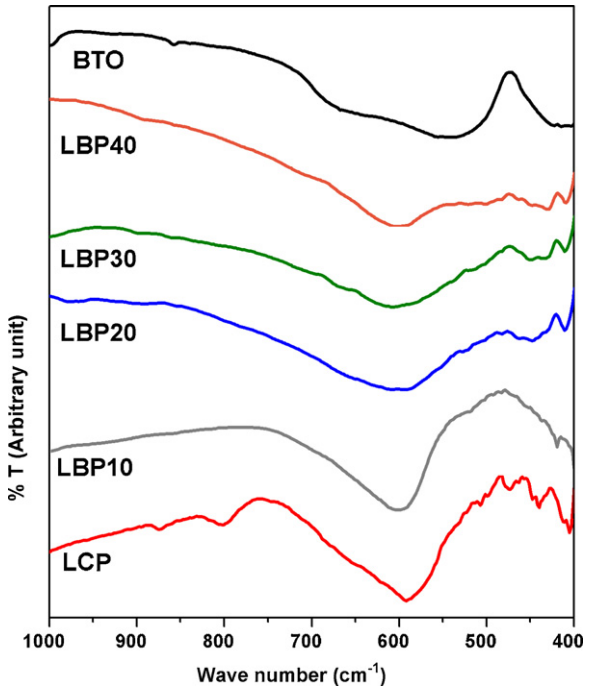

Fig. 2. IR spectra for LBP series.

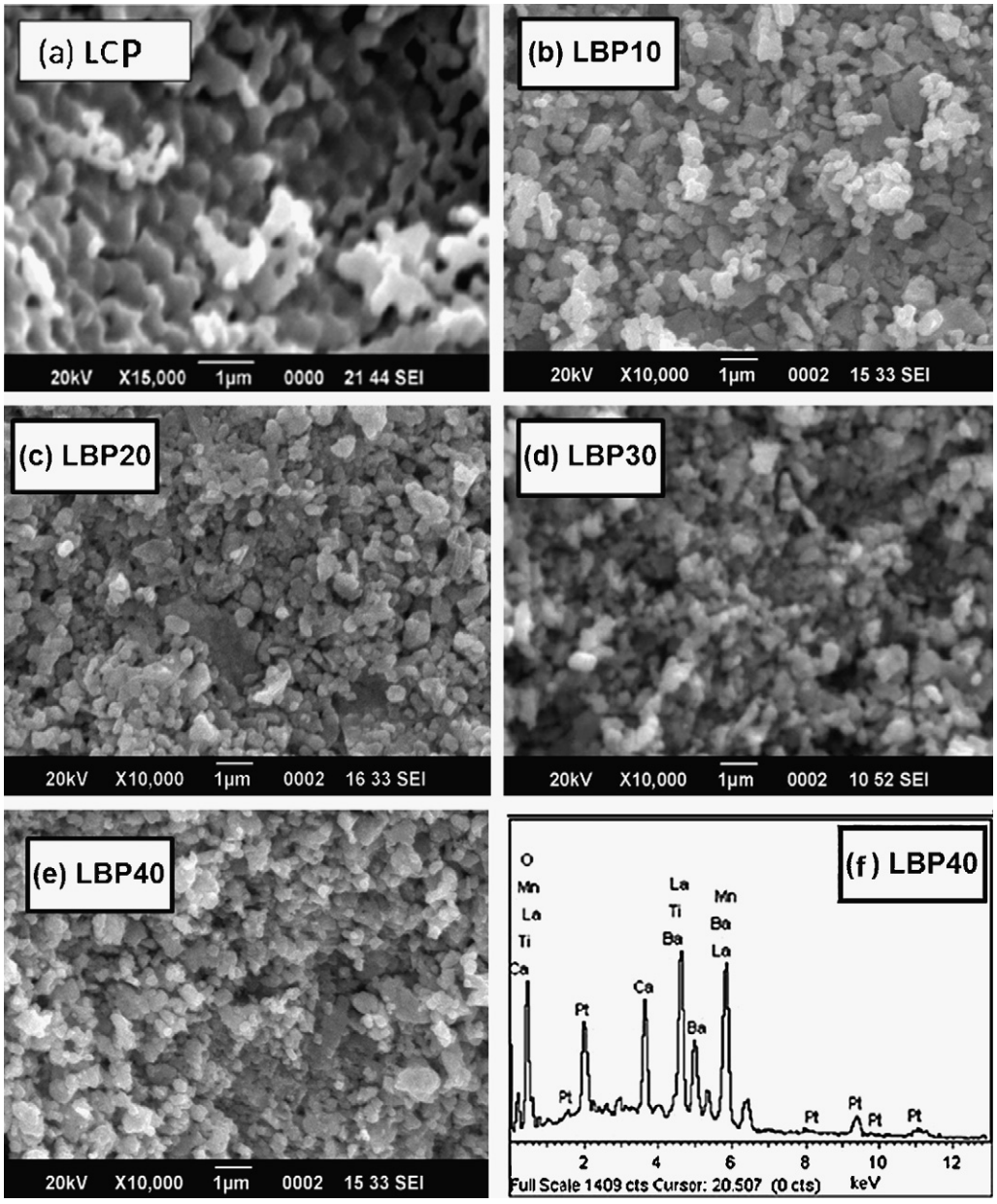

Fig. 3. SEM micrographs of (a) LCP, (b) LBP10, (c) LBP20, (d) LBP30, (e) LBP40 samples and (f) EDX result for LBP40 composite.

shift is observed, which supports the negligible interdiffusion between the phases.

3.1.3. SEM and EDX analysis

Fig. 3(a)–(f) depicts that the SEM images of different samples of LBP composite series along with EDX analysis for LBP40 sample. From this figure, it is evident that the grains of parent LCP are distinct and have well-defined boundaries. The pattern of grains in composites changes from parent LCP due to the presence of BTO phase, which have comparable grain size to that of LCP. This difference occurs due to the strain induced in the system because of presence of BTO grains. The strain induced in the system can be explained on the basis of distribution of grains of different sizes. These results reconfirm the coexistence of both types of grains. Fig. 3(f) shows the EDX pattern of LBP40 sample. Since manganese acetate has been taken as one of the starting materials for the preparation of LCP, a small amount of residual carbon is also found in the EDX data. The observation of Pt peaks in the EDX spectra come from the coating of platinum over the surface of sample.

3.2. AC susceptibility

The magnetic behavior of the samples of LBP series has been analyzed by studying temperature variation of real (χ') component of AC susceptibility as shown in Fig. 4. The PM to FM phase transition temperature which is known as Curie temperature (T_c) is determined from minimum point of $|d\chi'/Dt|$ versus temperature plot as given in Table 1. From this figure, it is evident that a sharp PM–FM transition occurs for LCP at $T_c \sim 270$ K, whereas a minute decrease in T_c is observed for composite samples. The inconsistency of T_c between the pure

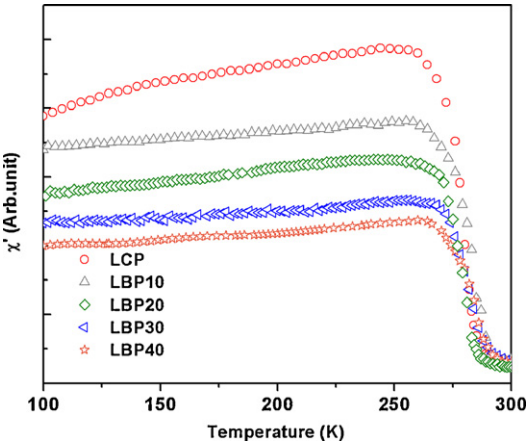

Fig. 4. Real part of AC susceptibility plotted as a function of temperature for LBP series.

and composite samples may be due to the different oxygen content in these samples. From these results we can argue that the magnetic coupling interaction within LCP grains has not been significantly altered because of BTO addition. The magnitude of AC susceptibility decreases successively by BTO addition as a result of decrease in the volume fraction of ferromagnetic LCP phase. Since BTO is nonmagnetic, the ferromagnetic order decreases with the decreasing fraction of LCP. With the increase in BTO content, the volume fraction of LCP decreases and because of this dilution effect, the value of χ' decreases.

3.3. Resistivity

Temperature dependent resistivities of LBP composite series is shown in Fig. 5 for the temperature range 5–300 K in the absence of magnetic field. Parent sample shows extrinsic MI transition at temperature $T_{MI} = 231$ K with an indistinct peak

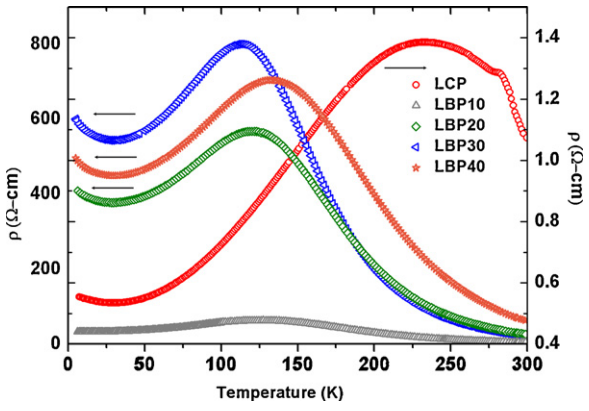

Fig. 5. Temperature variation of resistivity for LBP series in the temperature range 5–300 K in absence of magnetic field.

corresponding to intrinsic MI transition nearly at T_c; whereas all composite samples show hump type extrinsic transition only (ref. Table 1). It can be observed from the figure that the electronic conductivity is greatly altered by the formation of composite with enhanced upturn at low temperatures ($T \leq 35$ K). Also, the resistivity increases with the increase of BTO content up to $x_m \approx 0.30$, T_{MI} decreases and resistivity at x increases. But for $x = 0.40$, a reverse trend is observed, i.e. T_{MI} again increases with a small decrease in resistivity. The most remarkable feature observed in composite samples is decrease in T_{MI} with the increase of the GB effect whereas there is no significant change in T_c [16]. The reason behind the prominent extrinsic single peak behavior of these composite samples can be understood in terms of enhanced GB effect. The GBs and grain surfaces are in disordered and amorphous states due to the effect of broken bonds and symmetry breaking. Also, because of disruption in DE interaction these are in nonmagnetic and insulating states. On the basis of conduction, grain forms core shell structure and it is in FM phase. Hence, electronic scattering at GBs and surface increases the resistivity. In composite samples, presence of insulating state across the GBs causes an additional barrier in electronic conduction and increases the resistivity by several orders of magnitude.

Figs. 6(a)–(f) represents the temperature dependent resistivity of LBP composite series in presence and absence of 3 T magnetic field along with the corresponding MR. The resistivity data for the range 50–300 K has been fitted using percolation model [17] given by.

$$\rho(T) = \frac{4\rho_M\rho_I}{((3f-1)\rho_M + (2-3f)\rho_I) + [((3f-1)\rho_M + (2-3f)\rho_I)^2 + 8\rho_M\rho_I]^{1/2}}$$

where f is the metallic fraction, which is considered as a constant. ρ_M and ρ_I are resistivities in metallic and insulating region, respectively, which are given by $\rho_M(T) = \rho_0 + \rho_2 T^2$ [16] and $\rho_1(T) = \rho_\alpha T \exp(E_p/k_B T)$ [18], where ρ_0, ρ_2 are constants, E_p is the polaron formation energy, k_B is Boltzmann's constant and ρ_α is the resistivity coefficient.

It can be seen from Fig. 6 that this model gives a reasonable fit to the resistivity data in temperature range 50–300 K for the complete series as shown by solid red line. The obtained parameters are listed in Table 2. From Table 2, it is evident that $E_p/k_B T$ decreases after $x = x_m$, similar sequences have been observed in presence of magnetic field also. This is because of the fact that extrinsic behavior dominates till the threshold value thereby increasing the values of fitting parameters, which strongly depend on GBs. This also results in increase in activation energy of transport process of carriers. With the application of field, spin fluctuations are suppressed thereby decreasing E_p. The values of E_p/k_B are found to be in the range 1400–1900 K. Similar to previous findings the value of f is found to be ~0.5 for all the samples [17]. The value of goodness of fit, as defined by R^2 is found to be ~0.99 for all the samples.

Fig. 6(f) shows a sharp MR peak for parent LCP sample corresponding to intrinsic MI transition nearly at $T_c \sim 270$ K.

Table 2
Best fit parameters obtained using percolation model having temperature independent volume fraction for LBP series.

H (T)	ρ (Ω-cm)	$\rho_2 \times 10^{-4}$ (Ω-cm)	$\rho_\alpha \times 10^{-5}$ (Ω-cm K^{-1})	E_p/k_B (K)	f	R^2
LCP						
0	1.92	0.10	2.01	1705	0.403	0.999
	±0.05	±0.08	±0.31	±16	±0.069	
3	1.21	0.11	0.31	2078	0.400	0.998
	±0.03	±0.08	±0.03	±14	±0.059	
LBP10						
0	8.01	0.61	3.03	1695	0.498	0.992
	±0.37	±0.09	±0.12	±13	±0.069	
3	4.79	0.42	2.04	1764	0.502	0.988
	±0.39	±0.04	±0.16	±15	±0.060	
LBP20						
0	110.11	0.44	10.01	1844	0.499	0.987
	±10.03	±0.08	±0.03	±14	±0.060	
3	63.72	0.32	9.02	1851	0.499	0.995
	±9.03	±0.08	±0.03	±14	±0.059	
LBP30						
0	132.36	0.63	7.03	1774	0.498	0.997
	±10.08	±0.01	±0.01	±18	±0.060	
3	75.47	0.46	8.03	1795	0.501	0.997
	±8.13	±0.08	±0.03	±14	±0.049	
LBP40						
0	151.51	0.60	21.02	1963	0.498	0.994
	±9.32	±0.01	±0.12	±18	±0.079	
3	92.79	0.49	20.03	1968	0.502	0.993
	±8.21	±0.08	±0.33	±17	±0.060	

MR curve of the parent LCP sample shows a small intrinsic peak at T_c, whereas no such peak is observed for all the composite samples, indicating that for these samples there is no detectable contribution of the intrinsic component of MR. For composite samples, the magnitude of MR increases almost linearly with the decrease in temperature. These findings indicate that because of incorporation of BTO in LCP, the MR property of the samples becomes completely extrinsic in behavior which can be ascribed to the spin-polarized tunneling between GBs. These findings indicate that because of incorporation of BTO in LCP, the MR property of the samples becomes completely extrinsic in behavior. But for our $La_{0.67}Ca_{0.33}MnO_3$–$BaTiO_3$ composite series [5], we have found that the intrinsic MR decreases with BTO addition while extrinsic MR gets enhanced until a threshold condition is achieved and after this the trend is reversed. The MR values for present series are of larger values compared to the previous series; this enhancement of MR can be attributed to the enhanced and sharper GB effects which also makes the behavior extrinsic type. This is important to note that for this series we have obtained almost linear temperature dependent extrinsic MR at temperatures below T_c. This brings out the importance of grain size dependent study of the magneto-transport properties of manganites.

Fig. 7(a) shows the normalized resistivity as a function of temperature for LBP series. At sufficiently low temperature (∼35 K) a noticeable resistivity minimum is observed for all the samples, following an upturn on further decrease in temperature. This is another extrinsic effect commonly found in polycrystalline samples. A steeper low-temperature resistivity upturn has been observed in the presence composite series as compared to previous series [5], which is mainly due to reduction in grain sizes of both the phases. Resistivity in this region has been analyzed using model based on Coulomb blockade theory proposed by Sheng et al. [19]. In Fig. 7(b) solid lines show the best fit results for the samples using equation based upon Coulomb blockade model where symbols represent the experimental data points. The slope of the line represents the measure of charging energy [16]. It has been observed that this upturn in the resistivity increases with addition of BTO phase till x_m ($x = 0.30$) and again decreases for $x = 0.40$. When the grain size is small the energy barrier at sufficiently low temperature is quite large, so the charge carriers are inhibited from tunneling from grain to grain giving rise to a steeper rise in resistivity. As the average grain size decreases the contribution from Coulomb barriers increases and charge carriers find enough energy to tunnel through the grains and upturn becomes more significant as reported. The slope of individual fit is proportional to an electrostatic Coulomb energy barrier between the grains.

Fig. 8 shows the field dependent MR the range 0–3 T measured at 10 K. The overall MR value increases at all

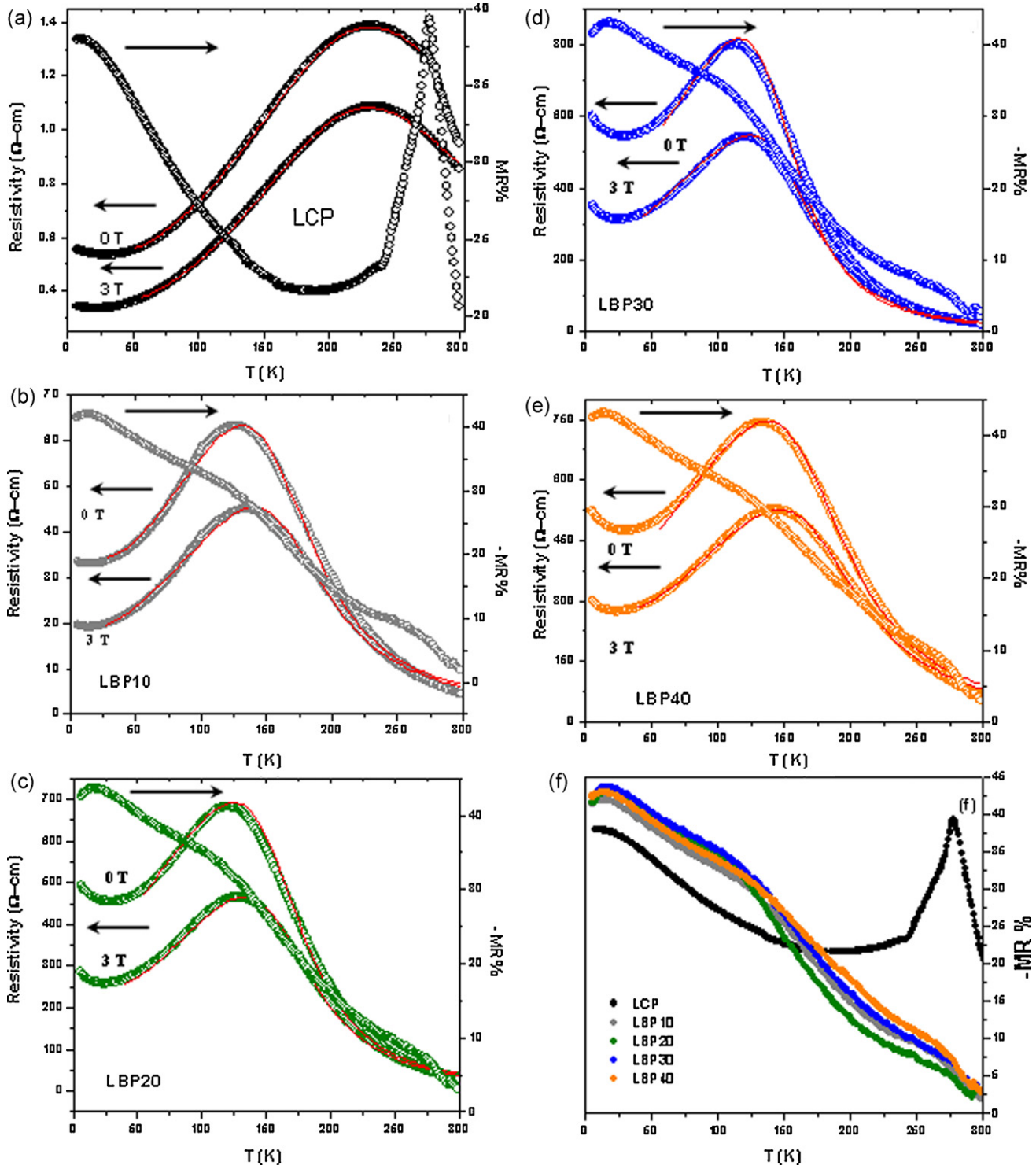

Fig. 6. (a)–(e) Temperature dependence of resistivity at 0 and 3 T and MR for LBP samples. Symbols are the experimental results and solid lines are the fittings using percolation model. (f) Temperature variation of MR of all samples at 3 T magnetic field.

applied fields. The maximum change in MR is observed at 0.5 T, where MR shows improvement from ∼7% to ∼28% for LBP20 sample. The prominent enhancement in MR can be stated as follows. It is because of the combined effect of decrease in grain size and addition of second phase. According to the model given by Anderson and Hasegawa [20] this combined effect enhances the disorder on grain surface and in the GB region. Hence, this upturn can be explained on the basis of Coulomb blockade and suppression of DE mechanism.

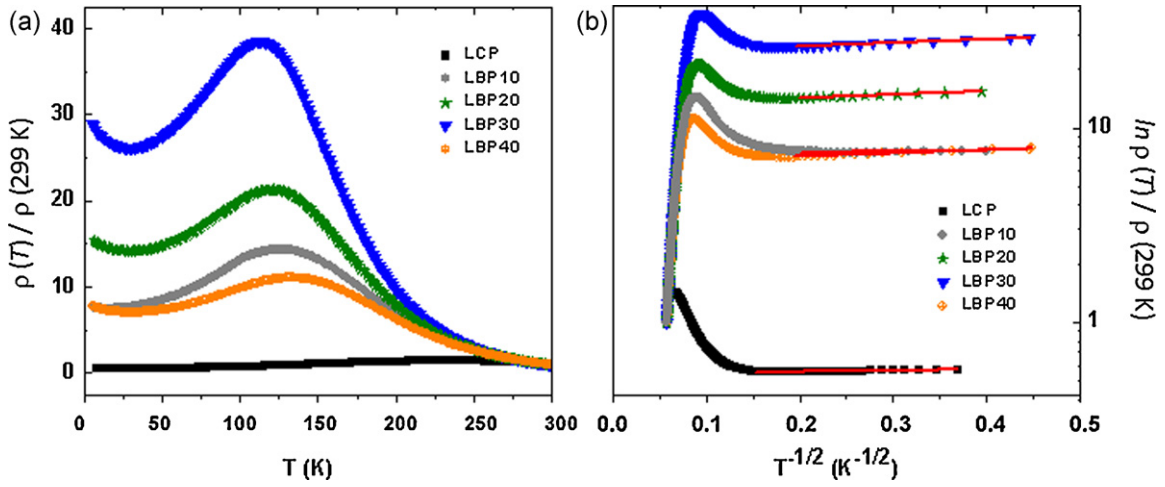

Fig. 7. Normalized reduced resistivity versus temperature for (a) LBP series; Plots of ln $p(T) = \rho(299\ \mathrm{K})$ versus $1/\sqrt{T}$, and (b) LBP series, where symbols represent the experimental data points, while best-fitted curves are shown by solid lines corresponding to percolation equation.

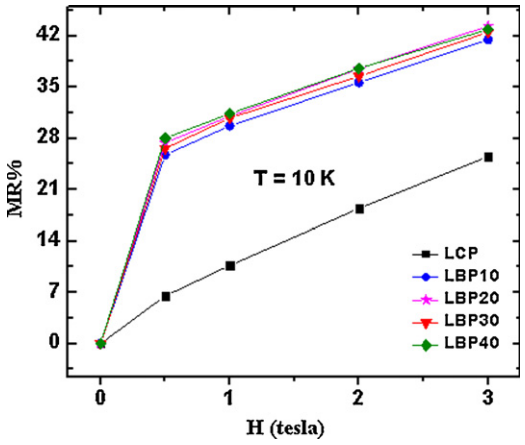

Fig. 8. Magnetic field dependence of MR in the range 0–3 T for LBP composites.

4. Conclusions

A series, $(1-x)La_{0.67}Ca_{0.33}MnO_3$ (LCP)–$(x)BaTiO_3$ (BTO), where LCP and BTO have been prepared by pyrophoric method, has been prepared for the systematic study on structural, magnetic and electrical properties. The main aim was to investigate the effect of grain size on physical properties of composites. While comparing these results with that of corresponding previous series [5], it has been observed that decrease in grain size as well as formation of composite promotes extrinsic behavior. The decoupling of T_{MI} and T_c is found to be function of both grain size and composite formation. Strain induced at the GBs generates a kind of electronic phase separation due to the breaking of Mn–O bonds and enhances the barrier across the GBs. All the composites of this series show a broad hump like transition in resistivity behavior, with percolation threshold at $x = 0.30$. There is a significant improvement in high field MR (at 3 T) as well as low field MR (at 0.5 T) in LCP–BTO composites when compared to parent sample.

Acknowledgements

S. Keshri gratefully acknowledges Department of Science and Technology (DST), for sanctioning the project. L. Joshi gratefully acknowledges Council of Scientific and Industrial Research for her fellowship. The authors would like to acknowledge Dr. R. Rawat, UGC–DAE Consortium for Scientific Research, Indore Center, India, for providing the MR facility. The authors are thankful to the members of Central Instrumentation Facility Lab, Birla Institute of Technology, Mesra for providing SEM and EDX facilities. The authors are also thankful to Mr. S.S. Rajput for fruitful discussions.

References

[1] C.N.R. Rao, B. Raveau, Colossal Magnetoresistance, Charge Ordering and Related Properties of Manganese Oxides, World Scientific, Singapore, 1998
[2] B. Vertruyen, R. Cloots, A. Rulmont, G. Dhalenne, M. Ausloos, P. Vanderbemden, Electrical transport and percolation in magnetoresistive manganite/insulating oxide composites: case of $La_{0.67}Ca_{0.33}MnO_3/Mn_3O_4$, Physical Review B 75 (2007) 165112–165116.
[3] P. Schiffer, A.P. Ramirez, W. Bao, S.W. Cheong, Physical Review Letters 75 (1995) 3336–3339.
[4] A. Moreo, S. Yunoki, E. Dagotto, Phase separation scenario for manganese oxides and related materials, Science 283 (1999) 2034–2040.
[5] S. Keshri (Shaw), L. Joshi, S.K. Rout, Influence of BTO phase on structural, magnetic and electrical properties of LCMO, Journal of Alloys and Compounds 485 (2009) 501–506.
[6] P. Li, S. Yuan, L. Liu, X. Wang, Y. Wang, Z. Tian, J. He, S. Yuan, K. Liu, S. Ying, C. Wang, Effect of grain boundary on electrical, magnetic and magnetoresistance properties in $La_{2/3}Ca_{1/3}MnO_3/CuMn_2O_4$ composites, Solid State Communications 146 (2008) 518–521.
[7] Z. Sheng, Y. Sun, X. Zhu, W. Song, P. Yan, Enhanced low-field magnetization and magnetoresistance in nano-MgO added $La_{2/3}Sr_{1/3}MnO_3$ composites, Journal of Physics D: Applied Physics 40 (2007) 3300–3306.
[8] X.S. Yang, Y. Yang, W. He, C.H. Cheng, Y. Zhao, Low-field magnetoresistance in $La_{0.7}Sr_{0.3}MnO_3/Ta_2O_5$ composites, Journal of Physics D: Applied Physics 41 (2008) 115009–115101.
[9] S.L. Young, T.C. Wu, L. Horng, C.H. Lin, H.Z. Chen, M.C. Kao, C.R. Ou, N.F. Shih, J.B. Shi, Magnetization processes of $(La_{0.7}Pb_{0.3}MnO_3)1-x(SiO_2)x$ composites, Journal of Superconductivity and Novel Magnetism 23 (2010) 953–955.

[10] T. Wang, X. Chen, F. Wang, W. Shi, Low-field magnetoresistance in $La_{0.7}Sr_{0.3}MnO_3/CuCrO_2$ composites, Physica B 405 (2010) 3088–3091.

[11] S. Hcini, S. Zemnia, A. Triki, H. Rahmouni, M. Boudard, Size mismatch, grain boundary and bandwidth effects on structural, magnetic and electrical properties of $Pr_{0.67}Ba_{0.33}MnO_3$ and $Pr_{0.67}Sr_{0.33}MnO_3$ perovskites, Journal of Alloys and Compounds 509 (2011) 1394–1400.

[12] P.K. Siwach, R. Prasad, A. Gaur, H.K. Singh, G.D. Varma, O.N. Srivastava, Microstructure–magnetotransport correlation in $La_{0.7}Ca_{0.3}MnO_3$, Journal of Alloys and Compounds 443 (2007) 26–31.

[13] S. Keshri, V. Dayal, Structural and electrical transport properties of nanosized $La_{0.7}Ca_{0.33}MnO_3$ sample synthesised by a simple low-cost novel route technique, Pramana 70 (2008) 697–704.

[14] V.S. Kolat, H. Gencer, M. Gunes, S. Atalay, Effect of B-doping on the structural, magnetotransport and magnetocaloric properties of $La_{0.7}Ca_{0.33}MnO_3$ compounds, Materials Science and Engineering B 140 (3) (2007) 212–217.

[15] K. Sadhana, T. Krishnaveni, K. Praveena, S. Bharadwaj, S. Murthy, Microwave sintering of nanobarium titanate, Scripta Materialia 59 (5) (2008) 495–498.

[16] P.T. Phong, N.V. Khiem, N.V. Dai, D.H. Manh, L.V. Hong, N.X. Phuc, Influence of Al_2O_3 on low-field spin-polarized tunneling magnetoresistance of $(1-x)La_{0.7}Ca_{0.3}MnO_3 + xAl_2O_3$ composites, Materials Letters 63 (3–4) (2009) 353–356.

[17] G.H. Rao, J.R. Sun, Y.Z. Sun, Y.L. Zhang, J.K. Liang, Magnetoresistance behavior of $La_{1-x}Ca_xMnO_3$ compounds, Journal of Physics: Condensed Matter 8 (1998) 5393–5400.

[18] G. Li, H.D. Zhou, S.J. Feng, X.J. Fan, X.G. Li, Z.D. Wang, Competition between ferromagnetic metallic and paramagnetic insulating phases in manganites, Journal of Applied Physics 92 (2002) 1406–1410.

[19] P. Sheng, B. Abeles, Y. Arie, Hopping conductivity in granular metals, Physical Review Letters 31 (1973) 44–47.

[20] P.W. Anderson, H. Hasegawa, Considerations on double exchange, Physical Review 100 (2) (1955) 675–681.